

8-1-2003

Communicating with microwave-propelled sails

Chaouki T. Abdallah

i. Sezi Bakim

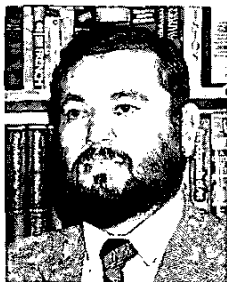
Edl Schamiloglu

Follow this and additional works at: http://digitalrepository.unm.edu/ece_fsp

Recommended Citation

Abdallah, Chaouki T.; i. Sezi Bakim; and Edl Schamiloglu. "Communicating with microwave-propelled sails." *IEEE Antennas and Propagation Magazine* 45, 4 (2003): 111-122. doi:10.1109/MAP.2003.1241321.

This Article is brought to you for free and open access by the Engineering Publications at UNM Digital Repository. It has been accepted for inclusion in Electrical & Computer Engineering Faculty Publications by an authorized administrator of UNM Digital Repository. For more information, please contact disc@unm.edu.



Naftali (Tuli) Herscovici
AnTeg
52 Agnes Drive
Framingham, MA 01901 USA
+1 (508) 788-5152
+1 (508) 788-6226 (Fax)
tul@ieee.org (e-mail)



Christos Christodoulou
Department of Electrical and
Computer Engineering
University of New Mexico
Albuquerque, NM 87131-1356 USA
+1 (505) 277-6580
+1 (505) 277-1439 (Fax)
christos@ece.unm.edu (e-mail)

Communicating with Microwave-Propelled Sails

İ. Sezi Bakım, Chaouki T. Abdallah, and Edl Schamiloglu

Department of Electrical and Computer Engineering
University of New Mexico
Albuquerque, NM 87131 USA

Tel: +1 (505) 277-0298; Fax: +1 (505) 277-1439; E-mail: chaouki@ece.unm.edu; edl@ece.unm.edu

Abstract

We describe a communication channel for a microwave-propelled sail, a novel concept for a deep-space scientific probe. We suggest techniques to recover the great loss introduced by the large distances, and we have conducted various simulations to understand the effects on the performance of the system. Possible disruption in the channel by high-energy solar flares, which increase the error in the estimation of the received signal, is accounted for. We developed the simulation for a full communication system on an additive white Gaussian noise (AWGN) channel, including the random-time solar-flare disturbance. We show that turbo codes can be exploited that perform very well at low SNRs and have high coding gain.

Keywords: Space vehicle communication; space vehicle antennas; space vehicle telemetry; Gaussian channels; Gaussian noise; codes; space vehicle propulsion

1. Introduction

1.1 Fundamentals of Microwave-Propelled Sails

Microwave-propelled sails were first introduced by the late Robert Forward as a continuation of his laser-driven sail concept [1, 2]. Missions beyond our solar system are impossible using present chemical-propellant-based propulsion systems, because the weight of the necessary fuel would be prohibitively excessive. The microwave-driven sail is man's only alternative to nuclear-fueled spacecraft for deep-space missions. Microwave-driven sails have the advantage that energy is expended to accelerate only the sail with its payload, not the propelling beam generator [3]. Interstellar flight requires speeds $\gg 100$ km/s (see Figure 1

for a depiction of the interstellar neighborhood). Of particular interest for scientists would be a mission to the region known as the Oort Cloud, composed of thousands of millions of comets extending beyond the Sun for a light year and beyond. Microwave-propelled sails are accelerated using beamed microwaves, and although electromagnetic waves (photons) have no mass, they do have both axial and angular momentum components. A reflected beam of light exerts a force F proportional to its power P via $F = 2P/c$, where c is the speed of light (3×10^8 m/s).

A severe limitation to beamed-microwave-driven sails is finding a material that can accommodate the severe mission constraints. The invention of ultra-light, strong, and high-temperature-compatible carbon material has made microwave-propelled sails a serious contender, because carbon does not melt: it sublimates at very high temperature [4]. Extremely high temperatures are needed

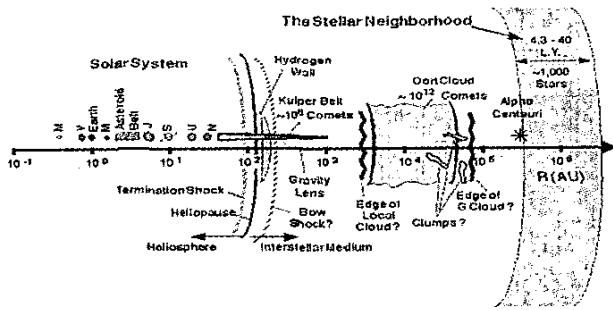


Figure 1. The solar system, hydrogen wall, Kuiper Belt, Oort Cloud, and stellar neighborhood [4].

because acceleration is strongly temperature limited, as is evident from the following consideration. The acceleration, a , from photon momentum produced by a power, P , on a thin film of mass m and area A is [5]

$$a = [\eta + 1] \frac{P}{MA} c, \quad (1)$$

where η is the reflection of the film of absorbtivity α , and M is the mass per unit area. (Absorbtivity is the ratio of absorbed power to incident power, transmissivity is the ratio of transmitted power to incident power, and emissivity is the ratio of emitted power to power emitted from a blackbody.) Carbon-fiber sail material with ~1% transmissivity can be produced. Thus, αP will be absorbed from the incident power on the film. This absorbed power must be radiated away from both sides of the film, which may be at different temperatures. We describe this power with an average temperature, T , and emissivity, ϵ , by the Stefan-Boltzmann law:

$$\alpha P = 2A\epsilon\sigma T^4, \quad (2)$$

where σ is the Stefan-Boltzmann constant ($5.67 \times 10^{-8} \text{ W/m}^2\text{-K}^4$). If we eliminate P and A , the sail acceleration is given by

$$a = \left(\frac{2\sigma}{c} \right) \left[\epsilon \frac{(\eta + 1)}{\alpha} \right] \left(\frac{T^4}{M} \right). \quad (3)$$

Clearly, the acceleration is strongly temperature dependent. All materials tested in early studies (Al, Be, Nb, etc.) could not be used for liftoff from Earth, since their melting temperature limited the achievable acceleration.

1.2 Sails and Interplanetary Missions – Scales and Distances

There are similarities between microwave-propelled sails and interplanetary missions. The channels in both cases are free space (except for transmission through the ionosphere and atmosphere), with almost no noise (unless we account for flares); the distance traversed is very large; and ultra-sensitive receivers are needed to extract the received signal.

Missions beyond the solar system have been successfully accomplished by Voyager 1 and 2. Voyager 1 is now the most-distant man-made object in the universe. It was at a distance of 12

billion kilometers (80 Astronomical Units (AU); 1 AU = $1.5 \times 10^{11} \text{ m}$) from the sun as of January, 2001. Voyager 2 was at 9.4 billion kilometers (62.7 AU) from the sun as of January, 2001. Voyager 1 is escaping from the solar system at a speed of about 3.6 AU per year ($\sim 17.1 \text{ km/s}$), 35° out of the ecliptic plane to the north. Voyager 2 is also escaping from the solar system at a speed of about 3.3 AU per year ($\sim 15.7 \text{ km/s}$), 48° out of the ecliptic plane to the south.

1.3 Sails and Interplanetary Missions – Communication Channel

Since the distance from a sail to the Earth is presumably large, by the time the signal arrives on Earth its power decreases considerably, so that we need ultra-sensitive receivers both on Earth and on the spacecraft (or the sail). The Deep-Space Network's (DSN's) receivers are sufficiently sensitive to receive signals of power -127.4 dBm or 10^{-16} W (Voyager 2's uplink received power) and -145.5 dBm or 10^{-18} W (Voyager 2's downlink received power) [6]. In our simulations, we have shown that we can receive powers of 10^{-13} or 10^{-14} W (depending on the transmitter power and the distance). The transmitted power of Voyager 2 is 72.6 dBm or 18 kW for the uplink, and 40.9 dBm or 12.3 W for the downlink, while the 70-meter antenna at the Goldstone Communication Complex is capable of transmitting a maximum of 400 kW . The microwave-propelled sail communication system we propose has greater coding gain than the Voyager mission, because we are using Turbo codes.

Encoding/decoding is very important, because coding gain compensates for the very weak received-signal power levels. The Voyagers' telemetry link also suffers from the noise in the communication channel, as do other deep-space links, causing bit errors. The rate of errors is reduced by error-correcting codes. Such codes increase the redundancy of the signal by increasing the number of bits transmitted relative to the information bit rate. The Golay encoding algorithm, used at the Jupiter and Saturn phase of the mission, required the transmission of one overhead bit for every information bit transmitted (100% overhead). Voyager had an experimental Reed-Solomon data encoder, expressly developed for the greater communication range of the Uranus and Neptune phase of the mission. The new Reed-Solomon encoding scheme reduced the overhead to about one bit in five (20% overhead), and reduced the bit-error rate in the output information from 5×10^{-3} to 10^{-6} [7]. In our simulations, we use Turbo codes that provide performance close to the Shannon limit [8]. The coding gain of Turbo codes is greater than traditional cyclic block codes and convolutional codes.

The DSN is able to transmit signals at L band, S band, X band, and Ka band, and can receive at S band and X band. Voyagers use S band for uplink, and S band and X band for downlink. Also, for the future missions, DSN is planning to use Ka band for both the uplink and downlink. We selected X band for both uplink and downlink for the microwave-propelled sail system simulations.

2. Communication System for a Microwave-Propelled Sail

A digital communication system includes a data source, encoding/decoding, multiple access, digital modulation, and an

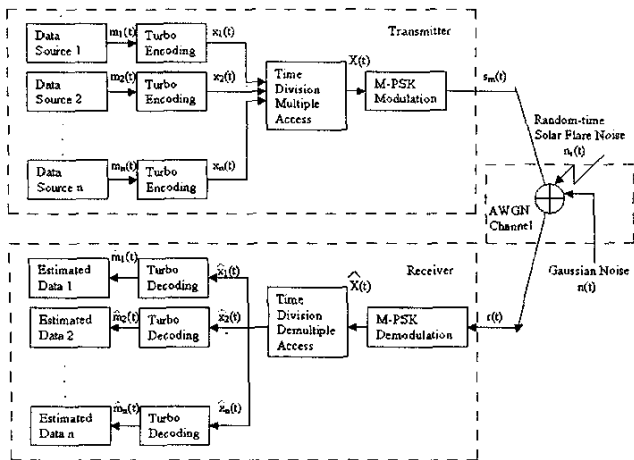


Figure 2. A communication system for a microwave-propelled sail.

appropriate channel. Commands to control the sail's operation and programming data, etc., are transmitted on the uplink to the sail, so we need to transmit more than one data stream at the same time. We use a multiple-access scheme in order to achieve this. Basically, we could use time-division multiple access (TDMA) and frequency-division multiple access (FDMA) in our system. We preferred to use TDMA in our system, because it was easier to implement in *MATLAB* simulations. We used M -ary phase-shift keying (M-PSK) modulation in our system. The M signal waveforms are represented as

$$s_m(t) = \text{Re} \left[g(t) e^{j2\pi(m-1)/M} e^{j2\pi f_c t} \right], \quad m = 1, 2, \dots, M, \quad 0 \leq t \leq T \quad (4)$$

$$= g(t) \cos \left[2\pi f_c t + \frac{2\pi}{M} (m-1) \right] \quad (5)$$

$$= g(t) \cos \frac{2\pi}{M} (m-1) \cos(2\pi f_c t) - g(t) \sin \frac{2\pi}{M} (m-1) \sin(2\pi f_c t), \quad (6)$$

where $g(t)$ is the signal pulse shape, and $\theta_m = 2\pi(m-1)/M$, $m = 1, 2, \dots, M$, are the M possible phases of the carrier that process the transmitted information [9]. Figure 2 presents a block diagram of the communication system we designed for a microwave-propelled sail.

2.1 Channel Model Description

The channel model of the communication system of a microwave-propelled-sail is one of the critical issues in our research. We use a free-space channel that is randomly disrupted due to solar flares and other effects of the solar wind. Unlike Earth-based communication systems that have definite noise characteristics and attenuations due to the channel, such as reflection, diffraction, scattering, fading, and interference, there is almost no noise in our proposed channel. The power levels decrease due to the free-space loss factor. We decided that the channel model that best fits our

proposed channel is the additive white Gaussian noise (AWGN) channel.

2.1.1 The Additive White Gaussian Noise (AWGN) Channel

We assume that digital information in the form of M signal waveforms $\{s_m(t), m = 1, 2, \dots, M\}$ is transmitted. Each waveform is transmitted within the symbol interval of duration T ; we consider transmission within the interval $0 \leq t \leq T$. The channel adds white Gaussian noise to the signal, as shown in Figure 3a. The received signal in the interval $0 \leq t \leq T$ may be expressed as

$$r(t) = s(t) + n(t), \quad 0 \leq t \leq T, \quad (7)$$

where $n(t)$ is a sample function of the additive white Gaussian noise (AWGN), with power spectral density $\Phi_{nn}(f) = \frac{N_0}{2}$ W/Hz.

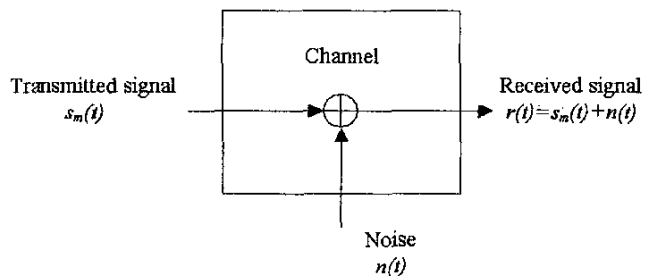


Figure 3a. The AWGN channel.

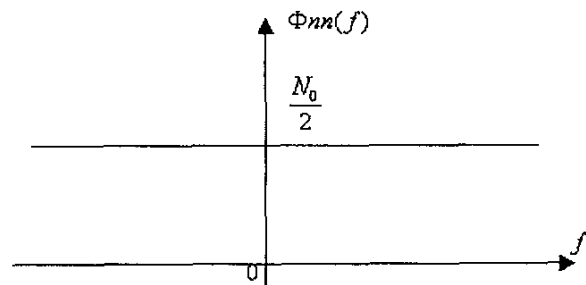


Figure 3b. The power density function of AWGN.

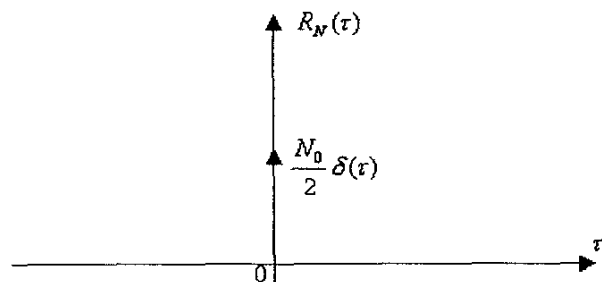


Figure 3c. The autocorrelation function of AWGN.

Typical characteristics of white Gaussian noise include the statistical independence of any two noise samples, a constant power spectral density

$$\Phi_{nn}(f) = \frac{N_0}{2} \text{ W/Hz}, \quad (8)$$

and an autocorrelation function

$$R_N(\tau) = \frac{N_0}{2} \delta(\tau), \quad (9)$$

as shown in Figures 3b and 3c.

2.2 Solar Activity

2.2.1 The Solar Cycle

Solar maximum is the term used for the maximum in solar activity that occurs approximately every 11 years, and the solar minimum is the lowest point of solar activity. The last solar maximum took place in 1989, and cycle 23's sunspot maximum was in 2000. Solar events can interact and interfere with each other, creating a very complex system. Their frequency varies with time. The smaller flares tend to follow the 11-year cycle, and peak at several tens of flares per day. The largest flares usually occur only a few times during the solar maximum. Sunspots increase with solar maxima and are relatively rare during quiet times. Coronal holes do not last as long during solar maxima as they do otherwise.

2.2.2 Solar Flares

A solar flare is a huge explosion in the solar atmosphere. It results in sudden bursts of particle acceleration, heating of plasma to tens of million degrees, and eruption of large amounts of solar mass [10]. Flares are believed to result from the abrupt release of the energy stored in magnetic fields in the zone around sunspots, and occur in the Sun's corona as the most violent form of solar activity. Solar flares are thought to originate from magnetic energy because of the very high energy output of the flares. They are the most powerful explosions in the solar system, releasing energies up to 20 million 100-megaton terrestrial nuclear bombs (amounting to 10^{25} Joules or 10^{32} ergs).

There are two types of flares: impulsive and gradual. Impulsive flares accelerate mostly electrons, with some protons. They last minutes or hours, and the majority appear near the solar equator. Impulsive flares occur at a rate of about 1000 per year during a solar maximum. Gradual flares accelerate electrons, protons, and heavy ions to near the speed of light, and the events tend to last for days. They occur mainly near the poles of the Sun, and occur about 100 times per year. This acceleration of solar-flare particles to extremely high energies involves all the different elements in the solar atmosphere. Ions of elements such as carbon, hydrogen, oxygen, neon, magnesium, silicon, and iron excited in this way end up in solar cosmic rays, also called solar energetic particles (SEPs).

2.2.3 Solar Flare in Our Channel Model

Impulsive solar flares last for a few minutes, and they have an energy $\sim 10^{32}$ erg. We included a moderate solar flare, of power 10^{15} W, in our simulation for 150 s (Δf is the bandwidth in the equations below):

$$\sigma^2 \Delta f = P_{noise} = 10^{15} \text{ W} \quad (10)$$

$$f_c = 7150 \text{ MHz (carrier frequency)} \quad (11)$$

$$f_s = 5f_c = 35750 \text{ MHz (sampling frequency)} \quad (12)$$

$$f_s = 2\Delta f \text{ (Nyquist rate)} \quad (13)$$

$$\Delta f = \frac{f_s}{2} = \frac{35750 \times 10^6}{2} = 17875 \times 10^6 \text{ s}^{-1} \quad (14)$$

$$\sigma^2 \Delta f = \sigma^2 \times 17875 \times 10^6 \text{ s}^{-1} = 10^{15} \text{ W} \quad (15)$$

$$\sigma \cong 236525 \quad (16)$$

We modeled the solar-flare noise as a Gaussian noise, with the calculated standard deviation given by Equation (16) occurring at a random time and lasting for 150 s.

2.3 Free-Space Loss

The received signal power in free space is inversely proportional to the square of the distance, d , between a transmitter and a receiver. Other parameters include transmitter-antenna gain, G_T ; receiver-antenna gain, G_R ; frequency, f ; and transmitter power, P_T . The relationship among these parameters and the received power, P_R , is given by

$$P_R = P_T G_T G_R \left(\frac{c}{4\pi f d} \right)^2 \text{ W}. \quad (17)$$

The distance between the transmitter and the receiver in the microwave-propelled sails is very large, from 10^1 to 10^6 AU ($1 \text{ AU} = 1.5 \times 10^{11} \text{ m}$). The largest attenuation in the communication systems of the microwave-propelled sails is due to the free-space loss, because the received signal power is inversely proportional to the square of the distance between the transmitter and the receiver. To limit the simulation time, in our model we used the scale distance from the Earth to the Sun, only (1 AU).

2.4 Turbo Codes

If the noise power is greater than the original signal power, after a certain value, the receiver can make incorrect decisions

about the transmitted signal. Shannon [8] proved that the probability of this error can be reduced to zero if the transmission rate does not exceed the capacity of the channel, C . If the average power of a signal is S over a channel of bandwidth B that adds additive white Gaussian noise (AWGN) with power N , the capacity is given by

$$C = B \log_2 \left(1 + \frac{S}{N} \right). \quad (18)$$

Turbo codes are a powerful class of error-correction codes that were introduced in 1993 by Berrou et al. [11], along with a practical algorithm. They have since been used in low-power applications, such as deep-space and satellite communications, and in interference-limited applications, such as third-generation cellular and personal-communication services. Turbo codes allow 10 dB possible coding gain on an AWGN channel with binary signaling, within 0.3 dB of the Shannon limit [12, 13].

2.4.1 Turbo Encoder

A turbo encoder consists of a parallel connection of two recursive systematic convolutional (RSC) encoders. These encoders receive the same information bits in different order. The interleaver is connected to the lower encoder, and this encoder receives the data after the interleaver permutes it. Before the information bits are fed into the lower RSC encoder, they are fed into the top RSC encoder, passed through an interleaver. The interleaver rearranges the input to the lower RSC encoder in order to emulate the randomized effect necessary for improved code performance, and makes turbo codes appear random. Multiplexing the systematic information with the parity information from both RSC encoders produces the output stream for a turbo encoder. One parity output is taken from each RSC encoder, and the systematic output of the turbo encoder is taken from the upper RSC encoder.

The output of an RSC encoder has quite a high Hamming weight because of its infinite impulse response. (A block code C comprises M code words $\{c_0, c_1, \dots, c_{M-1}\}$. Each code word is a one-to-one mapping to an input stream. A (n, k) block has a rate $r = k/n$, and $M = 2^k$ if binary. The number of bits with which the blocks differ is the Hamming distance, $v(c_i, c_j)$, between two code words. The smallest Hamming distance between code words is the minimum distance of a code $d_{\min} = \min_{i \neq j} v(c_i, c_j)$. The

Hamming distance between itself and the all-zero code word is the Hamming weight of a code word.) When both encoders produce outputs with low Hamming weights (occurring very rarely), turbo-code performance at low SNR is excellent. The Hamming weight of turbo codes is not very high, but the reason for their excellent performance is the reduced frequency of the low-weight code words. This allows turbo codes to perform better under low SNR, where low-weight codes are infrequent.

2.4.2 Turbo Decoder

The output of each constituent RSC encoder of a turbo code depends only on the last input bit, so the encoding process can be used as two joint Markov processes. The two Markov processes run on the same input data, so that turbo decoding can continue by

first independently estimating the process, then sharing information between both decoders. Therefore, the output of one decoder can be used as a priori information by the other decoder. To be able to use this, each decoder needs to produce soft-bit decisions, usually in the form of *log-likelihood ratios* (LLRs). The log-likelihood ratio a priori informs on the probability of a transmitted message bit as being 1 rather than a 0:

$$\Lambda_i = \ln \frac{P[m_i = 1/y]}{P[m_i = 0/y]}. \quad (19)$$

A soft-input, soft-output (SISO) decoder accepts input in the form of a priori information, and produces output in the form of a posteriori information (the SISO decoder). The inputs to the SISO decoder are systematic information, parity information, and a priori information, and the output is the log-likelihood ratio defined by Λ_i . The log-likelihood ratio of an SISO decoder can be expressed by

$$\Lambda_i = \frac{4a_i^{(s)} E_s}{N_0} y_i^{(s)} + z_i + l_i, \quad (20)$$

where $y_i^{(s)}$ is the current decoder's systematic input, z_i is the previous decoder's output, and l_i is newly obtained probability information. Decoding starts when the first decoder receives the first encoder's parity bit and the systematic channel observations. The first decoder produces the output log-likelihood ratio. Using that, the extrinsic information is obtained by subtracting the weighted systematic and a priori information for the second decoder. In the same manner, the extrinsic information is also obtained from the log-likelihood ratio of the second decoder. The message bits are estimated by making a hard decision on the de-interleaved output of the second decoder after the determined number of iterations.

2.4.2.1 Decoding Algorithms for Turbo Codes

An important algorithm that has been exploited successfully by turbo codes is the maximum a posteriori probability (MAP) algorithm. The MAP algorithm was first presented to the coding community in 1974 by Bahl, Cocke, Jelinik, and Raviv [14]. (It is also sometimes referred to as the BCJR algorithm, in honor of its discoverers). It is an algorithm for estimating random parameters with prior distributions. Sub-optimal approximations to the MAP algorithm have been developed to reduce the complexity of the system but not significantly reduce its performance. We describe these next [15]. Consider a recursive systematic convolutional code of constraint length K that encodes blocks of size N . The encoded information bits are $d = \{d_0, d_1, \dots, d_{N-1}\}$, and the noisy estimates of the encoded bits that the decoder receives are $y = \left\{ \left(y_0^{(s)}, y_0^{(p)} \right), \left(y_1^{(s)}, y_1^{(p)} \right), \dots, \left(y_{N-1}^{(s)}, y_{N-1}^{(p)} \right) \right\}$, where $y_k^{(s)}$ and $y_k^{(p)}$ are the received estimates of the systematic and parity bits, respectively. S_k is the state of the encoder at time k , where the state starts and ends in the all-zeros state

$$S_k = 0, \text{ for } k = 0, \dots, N. \quad (21)$$

The a posteriori probabilities (APPs) for each information bit, a 1 or 0, are produced by the MAP algorithm based on the received data from the channel. The a posteriori probability is expressed as

$$\Pr[d_k = i | y] = \sum_{S_k} \lambda_k^i(S_k) \quad (22)$$

where $\lambda_k^i(S_k)$ is the joint probability

$$\lambda_k^i(S_k) = \Pr[d_k = i, S_k | y] = \frac{\Pr[d_k = i, S_k, y]}{\Pr[y]} \quad (23)$$

The log-likelihood ratio can be calculated as

$$\Lambda(d_k) = \log \frac{\Pr[d_k = 1 | y]}{\Pr[d_k = 0 | y]} \quad (24)$$

Hard decisions are made by testing the sign of $\Lambda(d_k)$. If $\Lambda(d_k) > 0$, then $d_k = 1$; else $d_k = 0$. For 2^L possible states S_k , there will be a set of $2 \times 2^L = 2^{L+1}$ branch transition probabilities with a single γ , the probability of the encoder going from state S_{k-1} to a state S_k when a particular bit d_k is encoded. The decoding procedure can be written in several steps:

1. Initialize α

$$\alpha(S_0) = \begin{cases} 1 & \text{for } S_0 = 0 \\ 0 & \text{for } S_0 \neq 0 \end{cases} \text{ and } \alpha(S_k) = 0 \quad \forall k \neq 0 \quad (25)$$

2. Initialize index variable $k = 1$

3. Calculate γ_i and α_k for all states S_k

4. Increment k

5. Repeat 3) and 4) until $k = N$

6. Initialize β

$$\beta(S_N) = \begin{cases} 1 & \text{for } S_N = 0 \\ 0 & \text{for } S_N \neq 0 \end{cases} \text{ and } \beta(S_k) = 0 \quad \forall k \neq N \quad (26)$$

7. Initialize index variable $k = N - 1$

8. Calculate γ_i and β_k for all states S_k

9. Decrement k

10. Repeat steps 8) and 9) until $k = 0$

11. Calculate the log-likelihood ratio from

$$\Lambda(d_k) = \log \frac{\sum_{S_k} \sum_{S_{k-1}} \gamma_1 \left[\left(y_k^{(s)}, y_k^{(p)} \right), S_{k-1}, S_k \right] \alpha_{k-1}(S_{k-1}) \beta_k(S_k)}{\sum_{S_k} \sum_{S_{k-1}} \gamma_0 \left[\left(y_k^{(s)}, y_k^{(p)} \right), S_{k-1}, S_k \right] \alpha_{k-1}(S_{k-1}) \beta_k(S_k)} \quad (27)$$

The MAP algorithm is very difficult to implement, but performs the best for finding estimates of the a posteriori probability of the information bits. The large number of multiplications takes too much time. One solution is to perform the whole decoding in the logarithmic domain. In the logarithmic domain, multiplication operations are turned into addition operations: $\log(ab) = \log a + \log b$. The disadvantage of the log domain is that it makes the original addition operation more complex, as can be seen for the Jacobian logarithm:

$$\log(e^{x_1} + e^{x_2}) = \max(x_1, x_2) + \log\left(1 + e^{-|x_2 - x_1|}\right) \quad (28)$$

At the case where x_1 and x_2 are not close in value, the second term in Equation (28) is close to zero, and we can assume $\log(e^{x_1} + e^{x_2}) \approx \log\left(1 + e^{-|x_2 - x_1|}\right)$. This approximation is essential for the Max-Log-MAP algorithm, since it reduces the complexity of the decoder, and provides soft outputs that are inferior to those produced by the MAP algorithm because the second term in Equation (28) is ignored. We can write Equation (28) as $\log(e^{x_1} + e^{x_2}) = \max(x_1, x_2) + f_c(|x_2 - x_1|)$, where $f_c(|x_2 - x_1|)$ is a correction function. If this correction function is divided into all of the computations of $\log(e^{x_1} + e^{x_2})$, then the accuracy of the MAP algorithm would remain with the decoding occurring in the logarithmic domain. This algorithm is called the Log-MAP algorithm. Since the correction function operates in one dimension, it can be implemented in a lookup table indexed by $|x_2 - x_1|$. The Log-MAP provides basically the same performance as the MAP algorithm, but the complexity is less, since the lookup table is small.

The soft-output Viterbi algorithm (SOVA) is also a logarithmic-domain algorithm that performs soft-output decoding of convolutional codes. SOVA and Max-Log-MAP provide identical performance for hard decisions, whereas Max-Log-MAP performs a little better than SOVA for soft decisions. This is due to the lower complexity of SOVA. Max-Log-MAP and SOVA are suboptimal algorithms for easy implementation.

3. Simulation Results

3.1 Preliminary Code Checks

We simulated our proposed communication system for a microwave-propelled sail using *MATLAB*. We used the codes developed by Wu and Valenti for turbo encoding/decoding [16], and we developed the communication system including turbo encoding/decoding, TDMA, QPSK, on an AWGN channel, where a random-time large solar-flare noise was added. Our *MATLAB* code prompts the user to enter the following parameters:

- The decoding algorithm, Log-MAP or SOVA (default: Log-MAP)
- The frame size, information + tail (default: 400)
- The code generator matrix (default: $g = [07;05]$)
- Choose punctured or unpunctured (default: punctured)

- The number of iterations for each frame (default: 5)
- The number of frame errors to terminate (default: 15)
- Which M-ary PSK you want to use (default: 4-PSK or QPSK)
- The carrier frequency (default: 3 GHz)
- The E_b/N_0 (SNR) in dB (default: 2)

For all of the simulations, the channel was AWGN with given E_b/N_0 s. We used E_b/N_0 s of 1, 1.5, 2, 2.5 dB, which are the worst-case scenarios, and are not practical for deep-space communications. Considerable effort went into analyzing the performance of the system, and details can be found in [17]. In summary, the following aspects of the simulation were checked for their effects on the results:

- Iteration number: when the frame size, N , is small, three to five iterations are appropriate for the BER to converge, and more iterations bring little gain.

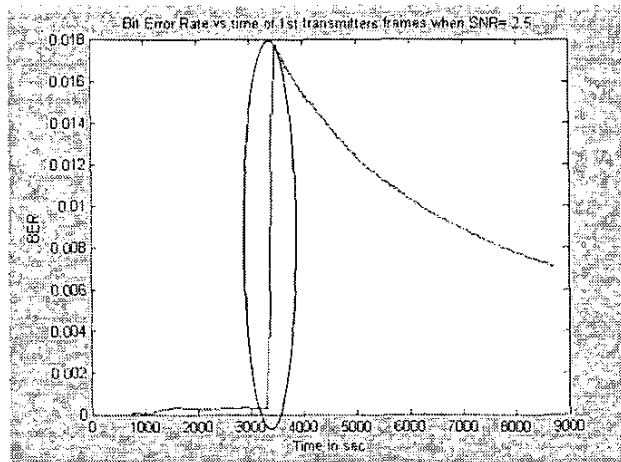


Figure 4a. The effects of a solar flare (time indicated by ellipse) on BER for first transmitter at an SNR of 2.5

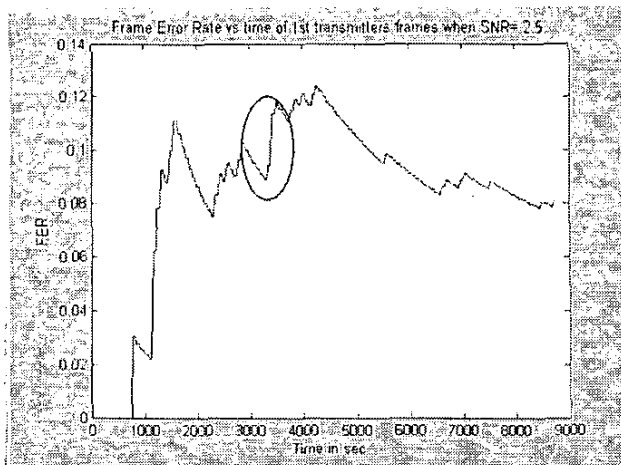


Figure 4b. The effects of a solar flare (time indicated by ellipse) on FER for first transmitter at an SNR of 2.5.

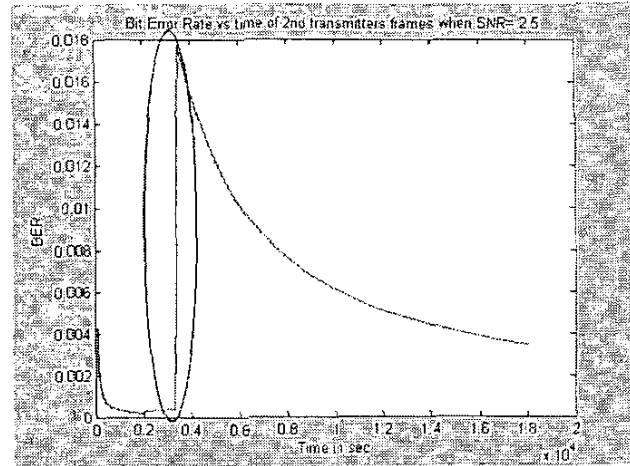


Figure 4c. The effects of a solar flare (time indicated by ellipse) on BER for second transmitter at an SNR of 2.5.

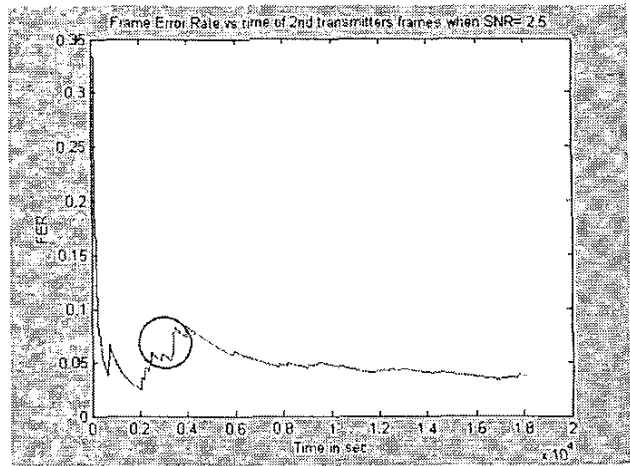


Figure 4d. The effects of a solar flare (time indicated by ellipse) on FER for second transmitter at an SNR of 2.5.

- Decoding algorithm: We used SOVA, the other decoding algorithm used in our simulation to see which of the decoding algorithms performed better. When we compared the results we found that the performance of the Log-MAP decoding algorithm was superior to the SOVA algorithm.
- Frame size: We ran the simulation with various frame sizes to understand the influence of the frame size on the performance of the system. We observed that for a fixed E_b/N_0 , increasing the frame size resulted in a lower BER.
- Code rate: We wanted to understand the effect of the code rate on the performance, so we ran the simulation with code rate = 1/3 (unpunctured). We concluded that decreasing the code rate from 1/2 to 1/3 gave more coding gain.
- Carrier frequency: We ran the simulation with carrier frequencies from 1 to 9 GHz, increasing in 2 GHz increments. The variation in frequency had only a slight effect on the performance in the range 1-9 GHz. We therefore used X band, 7150 MHz, for the uplink, and 8415 MHz for the downlink.

3.2 Effects of Solar Flare Noise

We had not considered the effects of solar flare noise thus far in our simulations. We now included this, and ran a full communication system's simulation (turbo encoding/decoding, TDMA, QPSK, AWGN channel with random-time solar-flare noise). The impulsive solar flare occurred at a random time and was active for 150 seconds (Figure 4). We used the following parameters: decoding algorithm, Log-MAP; frame size, 1024; generator matrix, $g = [07; 05]$; punctured, $r = 1/2$; number of iterations for each frame: 8; number of frame errors to terminate: 30; QPSK; carrier frequency: 7150 MHz; E_b/N_0 : 1, 1.5, 2, 2.5 dB; TDMA (two data sources transmitting frames). The great increase in both the BER and frame error rate (FER), as shown in the ellipses in Figure 4, was when the solar flare occurred. When the solar flare occurred a long time after the simulation begins, the BER and FER became very small, and the solar flare increased both BER and FER significantly, as seen in the figure. We also ran the simulation at lower SNRs, and concluded that small values of SNR (such as SNR = 1) were not suitable for the model, since both BER and FER were not low enough for reliable communications. When a solar flare occurred, the received signal was too large, and might harm the receiver. In order to protect the electronic circuits of the receiver and to have acceptable BER and FER, we decided to detect whether or not the solar flare occurred. If a solar flare was detected, power to the receiver was shut off. This protected the receiver and prevented the increase in both BER and FER. The data would then be recovered after the disturbance had passed (to be discussed below).

We next calculated the sums of the absolute value of bits in each received frame on an AWGN channel without the solar flare, so that we could compare these sums with the sums of frames including the solar-flare effect (Figures 5 and 6). For this simulation, we used the following parameters: decoding algorithm, Log-MAP; frame size, 1024; generator matrix, $g = [07; 05]$; punctured, $r = 1/2$; number of iterations for each frame, 8; number of frame errors to terminate, 30; QPSK; carrier frequency, 7150 MHz; E_b/N_0 , 1, 1.5, 2, 2.5 dB; TDMA (two data sources transmitting frames). We see that the sums of absolute values of bits in each received frame in Figure 5 is $\sim 1.5 \times 10^5$ and it got slightly bigger

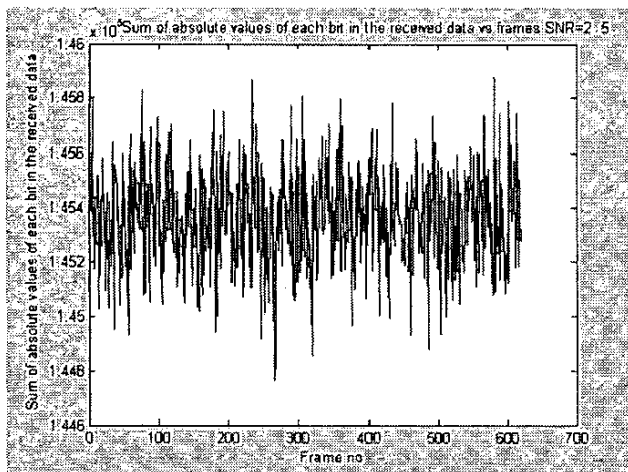


Figure 5a. The sums of the absolute value of bits in each received frame on an AWGN channel in the absence of a solar flare disturbance for SNR = 2.5.

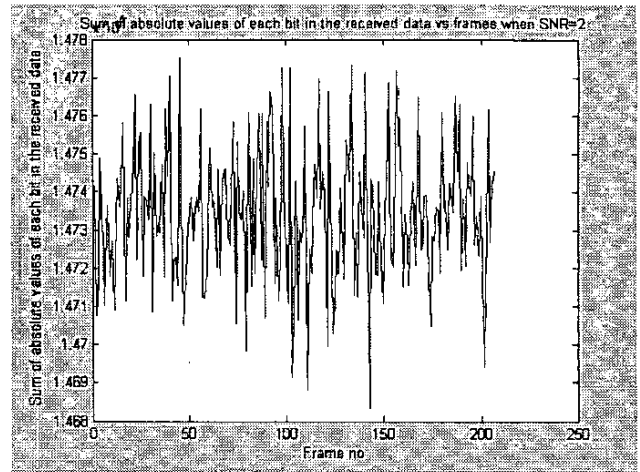


Figure 5b. The sums of the absolute value of bits in each received frame on an AWGN channel in the absence of a solar flare disturbance for SNR = 2.0.

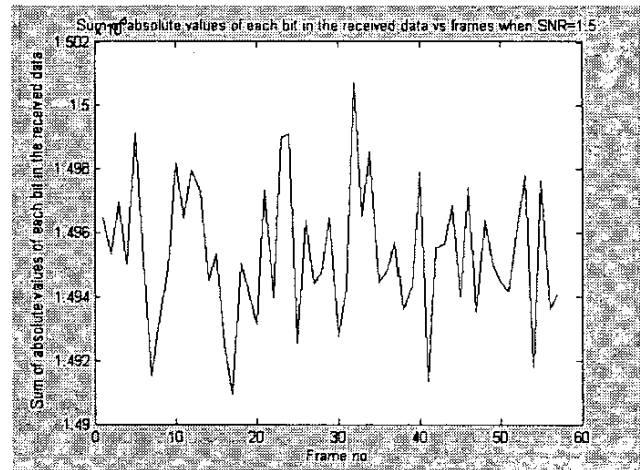


Figure 5c. The sums of the absolute value of bits in each received frame on an AWGN channel in the absence of a solar flare disturbance for SNR = 1.5.

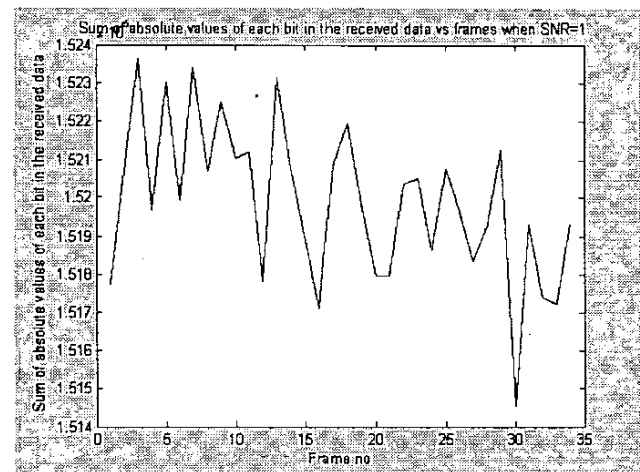


Figure 5d. The sums of the absolute value of bits in each received frame on an AWGN channel in the absence of a solar flare disturbance for SNR = 1.0.

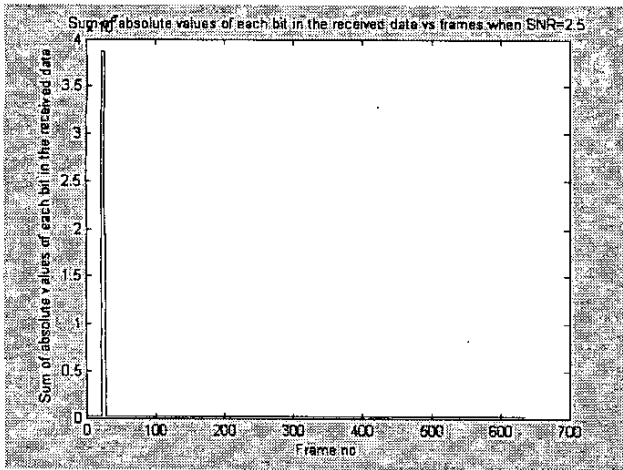


Figure 6a. The sums of the absolute value of bits in each received frame on an AWGN channel accounting for a solar flare disturbance for SNR = 2.5.

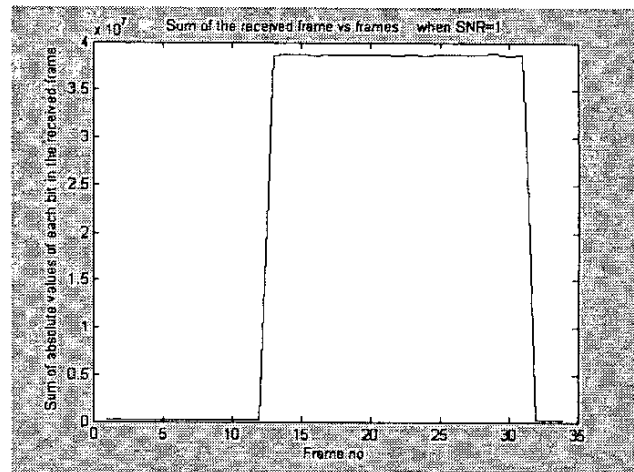


Figure 6d. The sums of the absolute value of bits in each received frame on an AWGN channel in the absence of a solar flare disturbance for SNR = 1.0.

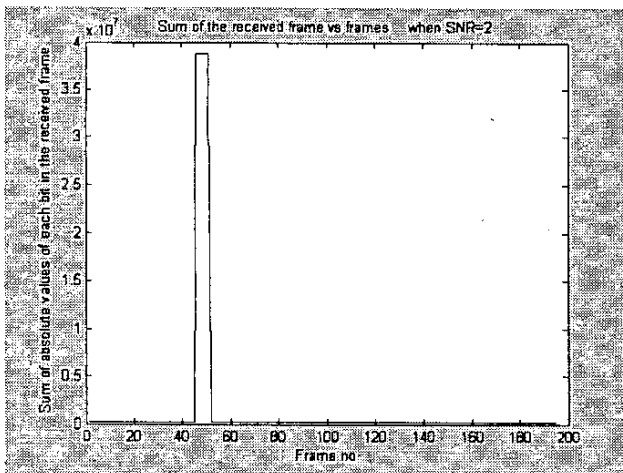


Figure 6b. The sums of the absolute value of bits in each received frame on an AWGN channel in the absence of a solar flare disturbance for SNR = 2.0.

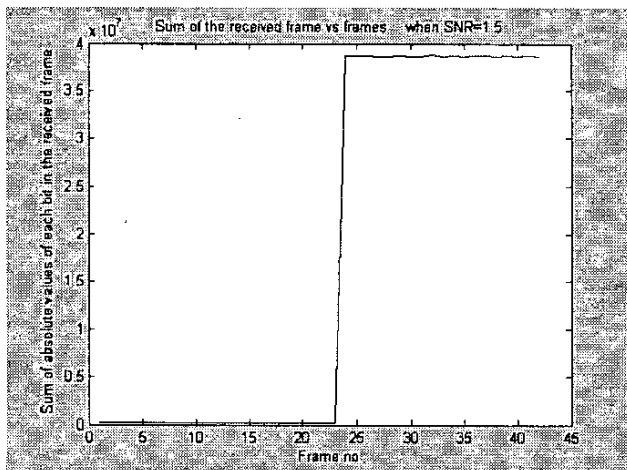


Figure 6c. The sums of the absolute value of bits in each received frame on an AWGN channel in the absence of a solar flare disturbance for SNR = 1.5.

as the SNR decreased, as expected, since low SNR corresponds to greater channel noise. We conclude that different SNRs in an AWGN channel without a random-time solar flare did not significantly change the sum of the received frames.

We then calculated the sums of the absolute value of the bits in each received frame on an AWGN channel with a random-time solar-flare noise (Figure 6). The great increase in the values of the summation was when the solar flare occurred. The sums of the absolute value of the bits in each received frame including the solar flare were up to $\sim 3.8 \times 10^7$, which was much greater than the summations without the solar flare ($\sim 1.5 \times 10^5$). We suggest this as an appropriate detector of the solar flare. We determined a threshold value of 2×10^5 for the sum, and decided that a solar flare occurred if the sum was greater than 2×10^5 . Since we now had a way to detect a solar flare, we could decide whether to receive and demodulate the received signal or not, and whether the solar flare occurred or not. If the summation was greater than this threshold, we assumed that the solar flare occurred, and did not demodulate those frames for 200 seconds. This protected the receiver and prevented BER and FER from significantly increasing. An impulsive solar flare lasts for a few minutes, so in the simulation we used the random-time solar flare for 150 s. We also recorded the numbers of the frames that we did not decode and transmitted those numbers at the end; the transmitter re-transmitted those frames to be decoded later. The proposed system used in our simulation model was as follows: Turbo encoding/decoding; TDMA; QPSK; AWGN channel including random-time solar-flare noise (detecting solar-flare noise, do not receive frames if flare occurred, send those frames at the end). We used the following for this simulation: decoding algorithm, Log-MAP; frame size, 1024; generator matrix, $g = [07; 05]$; punctured, $r = 1/2$; number of iterations for each frame, 8; number of frame errors to terminate, 30; QPSK; carrier frequency, 7150 MHz; E_b/N_0 , 1, 1.5, 2, 2.5 dB; TDMA (two data sources transmitting frames).

As can be seen in Figure 7, when a solar flare occurred (highlighted by the ellipses in the figure), we could not have reliable communications with the sail. The demodulated signal could be interpreted as a random signal. When we turned off the power and did not receive the frames, the BER and FER remained the

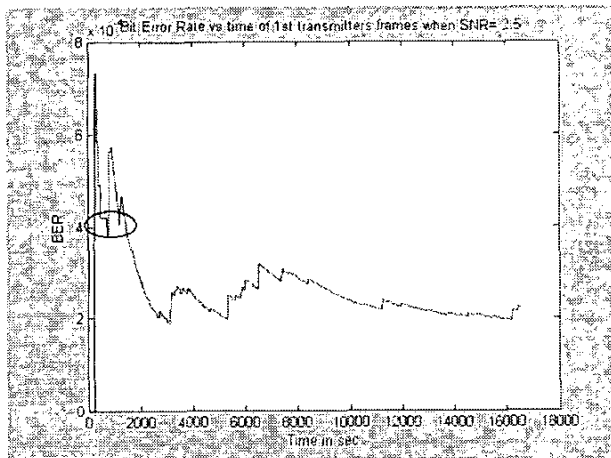


Figure 7a. The effects of a solar flare (time indicated by ellipse) on BER with the receiver powered off during the solar flare for first transmitter at an SNR of 2.5.

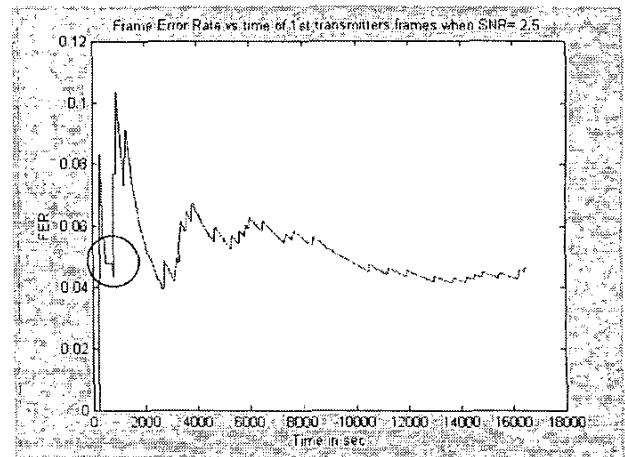


Figure 7b. The effects of a solar flare (time indicated by ellipse) on FER with the receiver powered off during the solar flare for first transmitter at an SNR of 2.5.

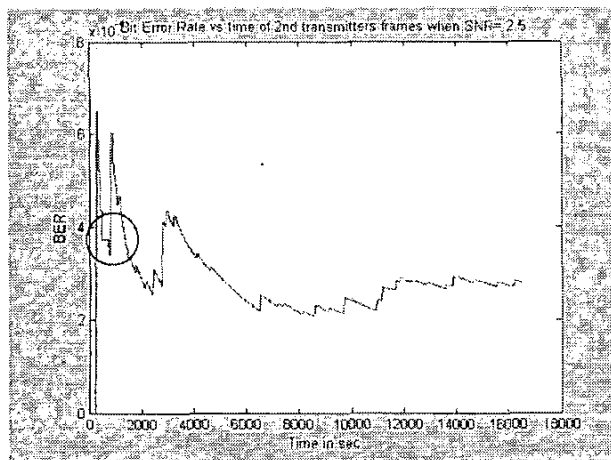


Figure 7c. The effects of a solar flare (time indicated by ellipse) on BER with the receiver powered off during the solar flare for second transmitter at an SNR of 2.5.



Figure 7d. The effects of a solar flare (time indicated by ellipse) on FER with the receiver powered off during the solar flare for second transmitter at an SNR of 2.5.

Table 1. Power calculations for uplink and downlink (original Voyager 2 parameters are noted with an asterisk).

| | Uplink | Downlink |
|---|---------------------------------------|--|
| 1. Transmitter RF Power | 72.55 dBm (18 kW)* | 40.90 dBm (12.30 W)* |
| 2. Transmitter Antenna Gain | 62.10 dBi* | 48.20 dBi* |
| 3. Space Loss (Freq = 7150 MHz, Range = 1.5×10^8 km) | -273 dB | -273 dB |
| 4. Turbo Coding Gain | 8 dB | 8 dB |
| 5. Receiver Antenna Gain | 34.60 dBi* | 74.01 dBi* |
| 6. Received Power (1+2+3+4+5) | -95.75 dBm (2.7×10^{-13} W) | -101.89 dBm (6.5×10^{-14} W) |

Table 2. Power calculations for a distance of 10^4 AU (original Voyager 2 parameters are noted with an asterisk).

| | Uplink | Downlink |
|--|--|--|
| 1. Transmitter RF Power | 72.55 dBm (18 kW)* | 40.90 dBm (12.30 W)* |
| 2. Transmitter Antenna Gain | 62.10 dBi* | 48.20 dBi* |
| 3. Space Loss (Freq = 7150 MHz, Range = 10^4 AU) | -353 dB | -353 dB |
| 4. Turbo Coding Gain | 8 dB | 8 dB |
| 5. Receiver Antenna Gain | 34.60 dBi* | 74.01 dBi* |
| 6. Received Power (1+2+3+4+5) | -175.75 dBm (2.7×10^{-21} W) | -181.89 dBm (6.5×10^{-22} W) |

Table 3: Power calculations for the maximum distance to have measurable received power levels (original Voyager 2 parameters are noted with an asterisk).

| | Uplink | Downlink |
|--|--------------------------|--|
| 1. Transmitter RF Power | 86.98 dBm (500 kW)* | 40.90 dBm (12.30 W)* |
| 2. Transmitter Antenna Gain | 62.10 dBi* | 48.20* dBi |
| 3. Space Loss (Freq = 7150 MHz, Range = 40709330322 km = 271.3955 AU) | -321.68 dB | -321.68 dB |
| 4) Turbo Coding Gain | 8 dB | 8 dB |
| 5) Receiver Antenna Gain | 34.60 dBi* | 74.01 dBi* |
| 6) Received Power (1+2+3+4+5) | -130 dBm (10^{-16} W) | -150.57 dBm (8.8×10^{-19} W) |

same as shown in the ellipses in the figure (unlike the original system) for a period of time (200 s in our simulation), and did not suffer from very high BER and FER.

3.3 Link Budget

Since the proposed mission for the microwave-propelled sail is in deep space, the power decreases considerably due to the free-space loss factor. We used the scale distance from the Earth to the Sun (1 AU) in our simulation model. For actual missions, we will need ultra-sensitive receivers and high-power transmitters. For the simulations, we used 18 kW transmitter power on Earth for the uplink, and 12.3 W transmitter power on the sail for the downlink. Table 1 summarizes the link budget for these parameters.

The received power for the uplink in our simulation was -95.75 dBm, which was reasonable, since the DSN's spacecrafts' ultras-sensitive receivers are capable of receiving signals less than -127 dBm. The received power for the uplink in our simulation was -101.89 dBm, also reasonable, since the DSN communication complexes' ultra-sensitive receivers are capable of receiving signals less than -145 dBm.

As discussed in the Introduction, scientists are interested in missions beyond the Kuiper belt to the Oort Cloud, which is composed of $\sim 10^{12}$ comets. Since some comets or asteroids may collide with the Earth in the future, scientists want to understand the structure of the Oort Cloud, and want to better understand comet formation and trajectories. The Oort Cloud is 10^4 AU away from Earth, so the free-space loss is very large. We calculated the received power levels when the distance between the sail and the Earth was 10^4 AU, and we found that the received powers were much less than the power levels DSN's ultra-sensitive receivers can receive and decode (Table 2). More-sensitive receivers, higher transmitter powers, and more efficient error-correcting codes are needed to be able to communicate with a sail that is 10^4 AU away from Earth.

We then calculated the greatest distance between the sail and the Earth in order to guarantee reliable communication using current technology. We used the maximum transmitter power of the DSN's 70-meter antenna in Goldstone (500 kW for the uplink transmitter and 12.3 W for the downlink transmitter). The maximum distance was 271.40 AU for suitable received power levels, $\sim 10^{-16}$ W for the uplink and $\sim 10^{-18}$ W for the downlink. The results are summarized in Table 3.

4. Conclusions

We designed and developed a simulation of a communication system for a microwave-propelled sail, including turbo encoding/decoding, TDMA, and QPSK on an AWGN channel where a random-time large solar flare was added to the channel. The large distances made the received signal power very low, and the flare made it difficult to receive and demodulate the data. Ultra-sensitive receivers and very efficient error-correcting codes with high coding gain, in addition to high transmitter powers, will be required to make this channel feasible.

In our simulations, we had an acceptable received power level for the scale distance of 1 AU. However, when we scaled the channel to the distance of the Oort Cloud (10^4 AU), we saw that the DSN's ultra-sensitive receivers would not be able to receive those power levels, since they were much less than the minimum acceptable levels. We calculated the maximum distance between the sail and the Earth for successful communications to be 271.40 AU. Clearly, additional development in technology will be required.

Future work will entail scaling this proposed channel to even greater distances. In so doing, the time delay of the signal inevitably becomes a factor to be included. For travel to distances as far as the Oort Cloud, more efficient codes should be developed, and higher transmitter powers will be required.

5. References

1. R. L. Forward, "Roundtrip Interstellar Travel Using Laser-Pushed Light Sails," *J. Spacecraft*, 1984, pp. 21, 187; R. L. Forward, "Starwisp: An Ultra-Light Interstellar Probe," *J. Spacecraft*, 1985, pp. 22, 345.
2. See, also, A. V. Pakhomov (ed.), *Beamed Energy Propulsion, Proceedings First International Symposium on Beamed Energy Propulsion*, AIP Conference Proceedings 664, Melville, NY, American Institute of Physics, 2003.
3. J. Benford, "Flight and Spin of Microwave-Driven Sails: First Experiments," Microwave Sciences Inc., Lafayette, CA, 2001.
4. Material invented and manufactured by Energy Science Laboratories, Inc., <http://www.esli.com>.

